Chiroptical Spectroscopic Determination of Molecular Structures of Chiral Sulfinamides: *t*-Butanesulfinamide

Ana G. Petrovic and Prasad L. Polavarapu*

Department of Chemistry, Vanderbilt University, Nashville, Tennessee 37235

Received: June 29, 2007; In Final Form: August 23, 2007

The absolute configuration of *t*-butanesulfinamide has been determined as (−)-(*S*) using three different chiroptical spectroscopic methods, namely, vibrational circular dichroism (VCD), electronic circular dichroism (ECD), and optical rotatory dispersion (ORD). Furthermore, the predominant conformation of this molecule is determined to have S═O and NH_2 groups staggered with respect to the three methyl groups and to have amine hydrogens in gauche orientation with respect to S═O. The quality of predictions obtained for vibrational properties, namely, vibrational absorption and VCD, is found to be satisfactory with the B3LYP functional and 6-31G* basis set. However, this basis set is found to be inadequate for obtaining reliable predictions of electronic properties, namely, electronic absorption and ECD, but a larger aug-cc-pVDZ basis set is found to provide satisfactory prediction of electronic properties. *t*-Butanesulfinamide serves as an example which invalidates the recommendation of using the 6-31G* basis set for molecules that exhibit the same sign for the long-wavelength ECD band and ORD. This molecule also emphasizes the importance of simultaneous investigation of ECD and ORD, and the use of multiple chiroptical spectroscopic methods, for reliable determination of molecular stereochemistry.

Introduction

Within the rich family of sulfoxides,[1,2] chiral sulfinamides are notable for their versatile utility as chiral building blocks. Sulfinamides have proven to be efficient chiral auxiliaries[3−6] and catalysts[7,8] in the enantioselective asymmetric synthesis of many organic compounds that are important for the development of active pharmaceutical ingredients and intermediates. Specifically, sulfinamides have been applied in the synthesis of enantiopure sulfinimines[1,4,9,10] as precursors for α- and *β*-amino acids,[4,10−12] α- and *β*-aminophosphonates,[13,14] and chiral amines.[15,16] Oxidation of sulfinamides yields[17] sulfonamides, which have been suggested[18] to have applications in medicinal chemistry. The sulfinamide derivative, peptidosulfinamide, has found application[19] for the development of HIV protease inhibitors.

The selective induction of chirality through asymmetric reactions necessitates not only the synthesis of enantiopure sulfinamides but also the reliable determination of their absolute stereochemistry. In recent years, chiroptical spectroscopic methods[20] are becoming invaluable tools for confident determination of absolute configuration and conformations of different types of chiral molecules. This accomplishment is made possible by the advances in instrumentation for experimental measurements, and in quantum theoretical methods for theoretical prediction, of chiroptical spectroscopic properties. However, the applicability of chiroptical spectroscopic methods for structural elucidation of chiral sulfinamides has not been explored in the literature. This paper addresses this deficiency through chiroptical spectroscopic studies of one of the simplest sulfinamides, namely, *t*-butanesulfinamide, **1** (Figure 1). The inexpensive synthesis and versatile utility of **1**, especially for generating chiral amines as key components of many pharmaceutical agents, are well documented.[8,21−25] The absolute configuration of **1** has been determined,[26] using the synthetic scheme employed, as (*R*)-(+)-**1**. The current study determines the absolute stereochemistry of **1** using three different chiroptical spectroscopic methods and examines whether the conclusions reached are in consensus with each other as well as with the literature configurational assignment.[26] The chiroptical spectroscopic methods[20] used here are vibrational circular dichroism (VCD), electronic circular dichroism (ECD), and optical rotatory dispersion (ORD). This study also examines the suitability of widely used 6-31G* and aug-cc-pVDZ basis sets for reliably predicting the chiroptical spectroscopic properties of **1**.

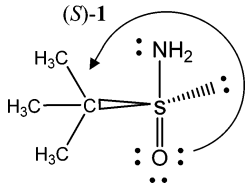

Figure 1. Chemical structure of *t*-butanesulfinamide (**1**).

Experimental Methods

Measurements. Both enantiomers of **1** have been purchased from Strem Chemicals and used as received. The vibrational absorption (VA) and VCD spectra were recorded in the 2000−900 cm^{-1} region using a commercial Fourier transform VCD spectrometer modified[27] to reduce the level of artifacts. The VCD spectra were recorded with 1 h data collection time at 4 cm^{-1} resolution. Spectra were measured in CH_2Cl_2 solvent at 50 mg/mL (0.413 M) for both enantiomers. The sample was held in a variable path length cell with BaF_2 windows and a path length of 135 μm. In the VA spectrum reported, the solvent absorption was subtracted out and the region of ∼1300−1250 cm^{-1} has been excluded due to interference from strong

* Corresponding author. E-mail: prasad.L.polavarapu@vanderbilt.edu.

10.1021/jp075077p CCC: $37.00
Published on Web 10/09/2007

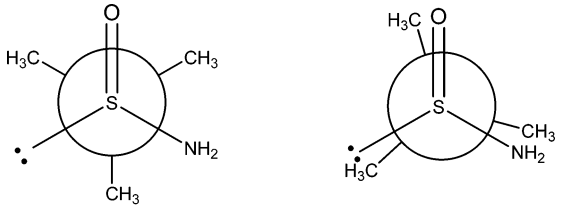

Figure 2. Newman projections of staggered and eclipsed forms of **1** used for conformational search.

solvent absorption. The baseline of the experimental VCD spectrum has been obtained by taking a difference between the VCD spectra of the two enantiomers and multiplying the result by 0.5. The concentration-dependent VA spectra have also been measured in the 50−10 mg/mL (0.413−0.0825 M) range in CH_2Cl_2 solvent to examine presence of dimers, but the evidence for dimer formation in the concentration range employed was not apparent.

The ECD spectra were recorded on a Jasco J720 spectrometer, using a 0.01 cm path length quartz cell. The electronic absorption (EA) spectra were recorded separately on a Cary-4E UV−vis spectrometer. The CH_2Cl_2 solvent background has been subtracted from the experimental spectra. The region below 205 nm is not displayed, in both experimental ECD and EA spectra, due to solvent interference. The optical rotations at six discrete wavelengths (633, 589, 546, 436, 405, 365 nm) have been measured with a 1 dm cell using an Autopol IV polarimeter. ECD and ORD measurements were obtained at a concentration of 10 mg/mL (0.0825 M) in CH_2Cl_2 solvent.

Calculations. The conformational search has been performed for **1** with (*S*)-configuration (Figure 1) by starting with staggered and eclipsed forms (Figure 2). The set of initial conformations has been generated by incremental 60° rotation of the amine group for both staggered and eclipsed forms given in Figure 2. The optimization of all of the initial structures has been carried out with the B3LYP functional and 6-31G* basis set. The eclipsed conformations are unstable as they converged to staggered conformations. Two stable conformations, both in the staggered form, have been identified (Table 1, Figure 3) for **1**, and these conformations have been further optimized with the aug-cc-pVDZ basis set. VA, VCD, EA, ECD, and ORD properties have been calculated with both 6-31G* and aug-cc-pVDZ basis sets, at the respective optimized geometries, for the two stable conformers. All calculations were undertaken with the Gaussian 03 program[28] using the B3LYP functional and 6-31G* and aug-cc-pVDZ basis sets.

The theoretical VA and VCD spectra were simulated with Lorentzian band shapes and 5 cm^{-1} half-width at half-peak height. The 6-31G* predicted vibrational frequencies are normally higher than the corresponding experimental vibrational frequencies, and therefore, the calculated frequencies have been scaled with a factor[29] of 0.9613. No such scaling has been used for the vibrational frequencies obtained with the aug-cc-pVDZ basis set.

The theoretical EA and ECD spectra were simulated from the first 30 singlet → singlet electronic transitions using Lorentzian band shapes and 20 nm half-width at half-peak height. Rotational strength values, calculated with velocity representation, have been used for the ECD spectral simulations. The EA spectral intensities are derived from dimensionless oscillator strengths. The peak extinction coefficient of the *i*th band, ϵ_i^0 (in $L \cdot mol^{-1} \cdot cm^{-1}$), is related to oscillator strength, f_i, as $\epsilon_i^0 = 7.369 f_i(\lambda_i^2/\Delta_i)$ where Δ_i is the half-width at half-height of the Lorentzian band.

Results and Discussion

Comparison of the Gibbs free energies of two stable conformers (Table 1) indicates that conformation 1 has lower energy and is significantly more populated than conformation 2. To evaluate the influence of solvent on the stability of these conformers, geometries of these two conformers have also been optimized with aug-cc-pVDZ basis set in CH_2Cl_2 solvent using the PCM model as implemented in Gaussian program.[28] However neither the geometries nor relative electronic energies are influenced significantly in the presence of solvent (see Table 1). The main difference among these two conformers is in the orientation of amine hydrogens with respect to the S═O group. Both amine hydrogens are gauche to S═O in conformer 1, while one amine hydrogen is trans to S═O in conformer 2. Structural parameters of the optimized structures (Figure 3) are summarized in Table 1.

The comparison between experimental and theoretical VA and VCD spectra of **1** in the 900−1800 cm^{-1} range is displayed in Figure 4. Panel A displays the comparison between the experimental VA spectrum and theoretical VA spectra for both conformers of **1**. A satisfactory qualitative agreement between the predicted VA spectrum of conformer 1 and the experimental VA spectrum can be seen, at both basis set levels. Specifically, the 10 labeled bands in Figure 4 correlate qualitatively well both in frequency positions and relative intensities. The agreement is much less satisfactory when the experimental VA spectrum is compared with the theoretical VA spectrum predicted for conformer 2. This observation can be used to suggest that the negligible population predicted for conformer 2 in vacuum may not have been changed by the solvent used for experimental measurements. On the basis of the predicted

TABLE 1: Dihedral Angles, Bond Lengths, Gibbs Free Energies, and Relative Populations of Two Optimized Conformers of 1

	conformer 1			conformer 2		
	6-31G*	aug-cc-pVDZ		6-31G*	aug-cc-pVDZ	
parameter[a]	vacuum	vacuum	PCM model	vacuum	vacuum	PCM model
D(O−S−N−H)	−34.08	−31.37	−32.73	169.49	171.49	158.18
D(N−S−C−C)	−59.25	−57.51	−57.50	−61.76	−59.61	−60.82
D(O−S−C−C)	54.75	55.23	56.08	49.64	50.61	49.97
R(O···H(N))	2.74	2.70	2.74	3.47	3.48	3.46
R(O···H(N))	3.04	3.05	3.06	2.88	2.87	2.99
E	−687.171245	−687.244980	−687.249390	−687.163784	−687.229870	−687.236404
G	−687.050044	−687.117780		−687.043572	−687.112372	
relative populations	0.999	0.997		0.001	0.003	

[a] *D* = dihedral angle (deg); *R* = distance (Å); *E* = electronic energy in hartrees; *G* = Gibbs energy in hartrees; PCM model calculations were done with CH_2Cl_2 solvent; see Figure 3 for atom labels.

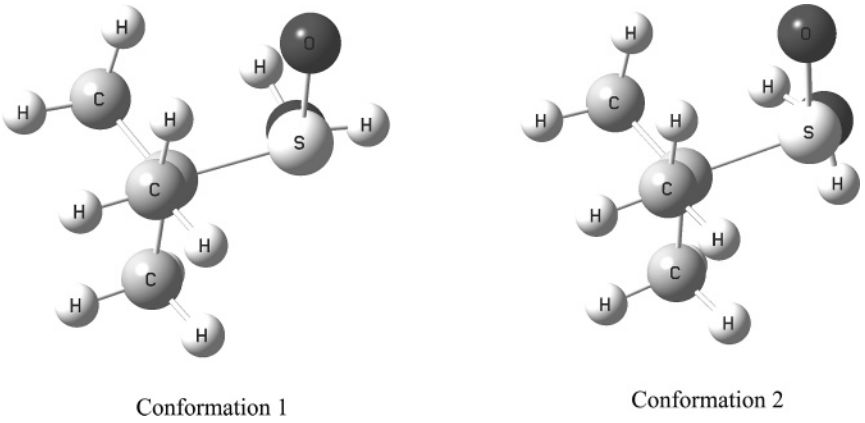

Figure 3. Structures of the two converged conformers.

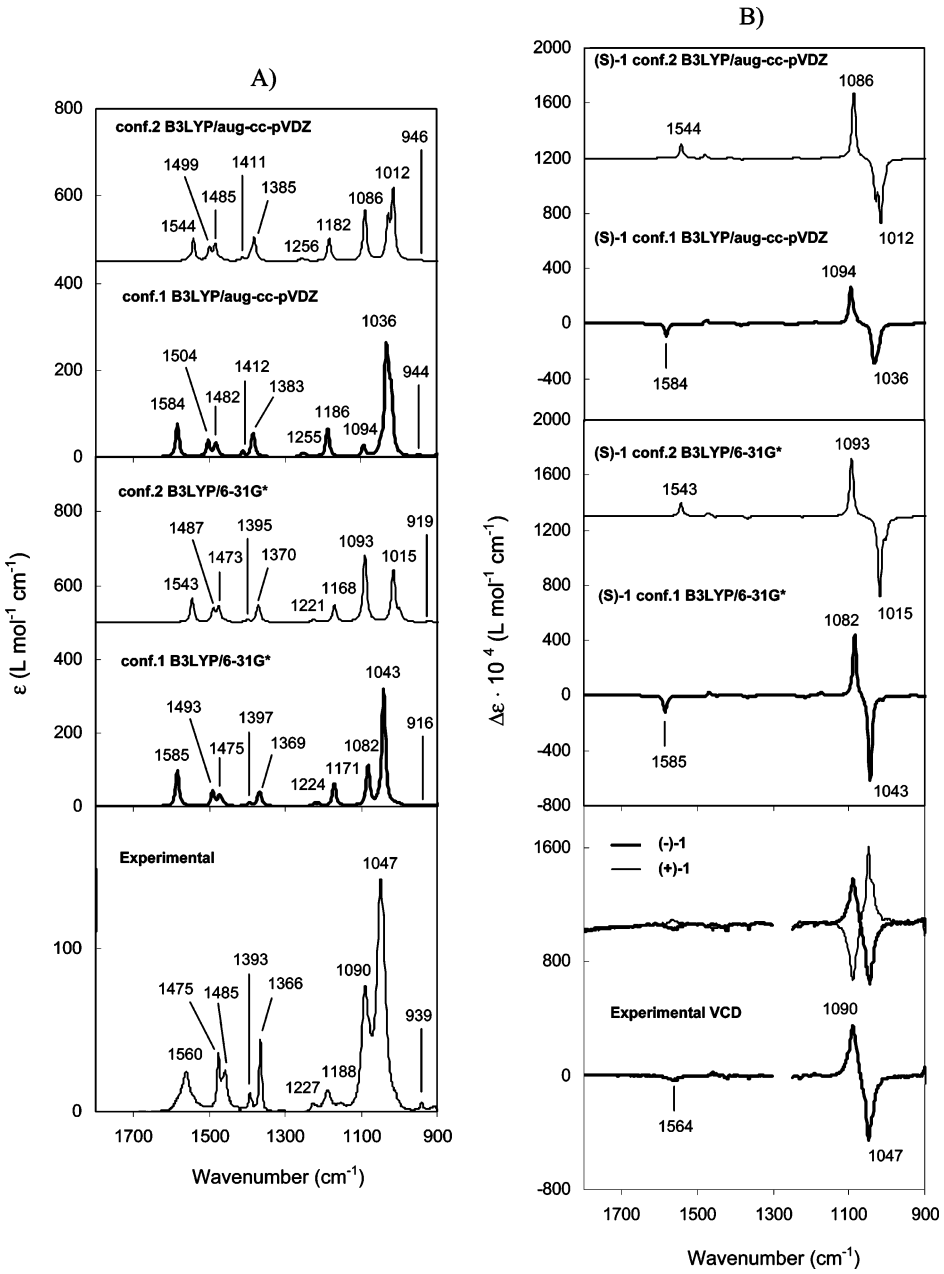

Figure 4. Comparison of VA (A) and VCD (B) spectra between (−)-**1** and both conformers of (*S*)-**1** at the 6-31G* and aug-cc-pVDZ basis sets.

vibrational displacements for conformer 1, the vibrational origins of 10 bands in the mid-infrared regions are summarized in Table 2.

The experimental VCD spectra, displayed in panel B of Figure 4, indicate three VCD bands with expected mirror images for the two enantiomers of **1**: a negative VCD couplet (negative

TABLE 2: Vibrational Origins of Mid-Infrared Bands Predicted with B3LYP Functional and 6-31G* and aug-cc-pVDZ Basis Sets for Conformer 1 of (*S*)-(−)-1[a]

frequency (cm^{-1})				
exptl	6-31G*	aug-cc-pVDZ	VCD sign	vibrational origin
939	916	944		C−C−C bending modes
1047	1043	1036	(−)	S═O bond stretching coupled with some NH_2 twisting
1090	1082	1094	(+)	NH_2 twisting coupled with some S═O bond stretching
1188	1171	1186		S−C bond stretching
1227	1224	1255		C−C−C bending modes coupled with C−C bond stretching
1366	1369	1383		methyl group bending modes
1393	1397	1412		
1485	1475	1482		
1475	1493	1504		
1560	1585	1584	(−)	NH_2 scissoring

[a] Vibrational frequencies predicted with 6-31G* basis set were scaled with 0.9613.

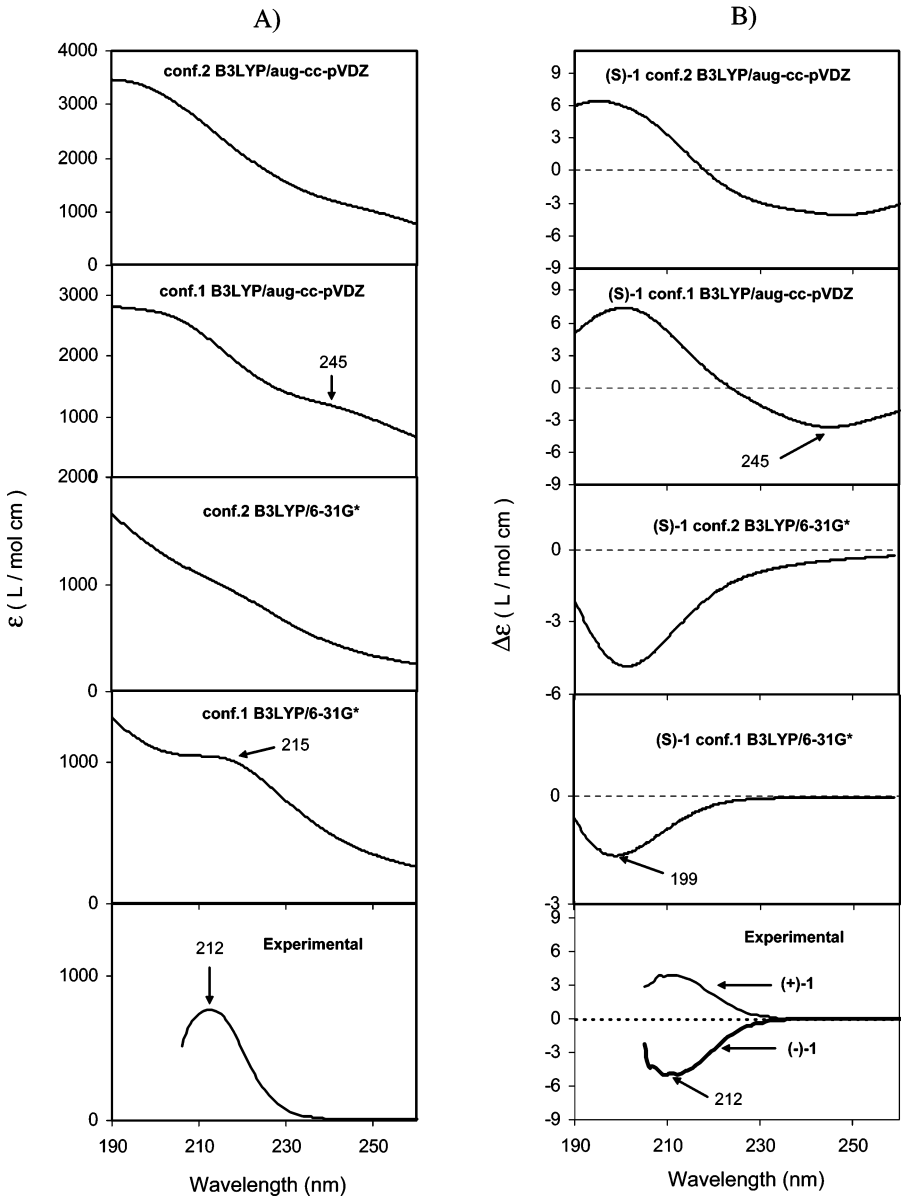

Figure 5. Comparison of EA (A) and ECD (B) spectra between (−)-**1** and both conformers of (*S*)-**1** at the 6-31G* and aug-cc-pVDZ basis sets.

VCD at 1047 and positive VCD at 1090 cm^{-1}) and a negative VCD band at 1564 cm^{-1} for (−)-**1**. The configurational assignment relies on the agreement of these three VCD bands between experimental and predicted VCD spectra. In the predictions obtained with the aug-cc-pVDZ basis set, the VCD couplet at (−)1036/(+)1094 cm^{-1} and a weak negative VCD band at 1584 cm^{-1} for conformer 1 of (*S*)-**1** correlate well with the couplet at (−)1047/(+)1090 cm^{-1} and a weak band at (−)-1564 cm^{-1} in the observed VCD spectrum of the (−)-**1**. The vibrational origin (Table 2) of the predicted VCD couplet is S═O bond stretching coupled with NH_2 twisting, whereas that of the higher frequency negative VCD band is NH_2 scissoring. The qualitative agreement with experimental VCD spectra is equally good for predictions with the 6-31G* basis set, as it is

with the aug-cc-pVDZ basis set, for conformer 1 of (*S*)-**1**. Quantitatively, the aug-cc-pVDZ basis set predictions provide a slightly better intensity reproduction of the dominant low-frequency couplet. Although the experimental VCD signs of the dominant couplet are also reproduced in the calculated spectrum for conformer 2, the sign of the high-frequency experimental VCD band is not reproduced in the calculated spectrum for conformer 2. In the higher frequency region where (−)-**1** exhibits a negative VCD signal, a positive VCD signal at 1544 cm^{-1} is predicted for conformer 2 of (*S*)-**1**. This predicted VCD signal also originates from NH_2 scissoring, and its mismatch in sign with the experimental observation indicates that conformer 2 is not dominant. Overall, the VCD spectra predicted with both basis sets provide evidence for the assignment of absolute configuration as (*S*)-(−)-**1**, with conformer 1 being dominant.

Larger discrepancies are noted in the theoretical results obtained with two chosen basis sets for ECD and ORD spectra, unlike in VA and VCD spectra. Figure 5 displays the correlation between experimental and predicted EA and ECD spectra. In panel A, the observed EA band at ∼212 nm seems to correspond to the predicted band for conformer 1 at ∼215 nm with 6-31G* basis set and predicted shoulder band at ∼245 nm with the aug-cc-pVDZ basis set. The EA spectrum predicted with the 6-31G* basis set for conformer 2 does not show a well-defined maximum, whereas that with the aug-cc-pVDZ basis set shows a shoulder at ∼245 nm, as for conformer 1. However, both conformers of (*S*)-**1** are predicted with the 6-31G* basis set to display (Figure 5B) a negative ECD band at ∼199 nm, which qualitatively matches the observed negative ECD band of (−)-**1** at ∼212 nm. The ECD spectra predicted with the aug-cc-pVDZ basis set for both conformers of (*S*)-**1** contain a negative band at 245 nm which correlates with the negative experimental ECD band at 212 nm of (−)-**1**. The aug-cc-pVDZ predicted ECD spectra also show a positive going ECD band at shorter wavelength, but a corresponding band in the experimental spectrum is not seen. The correlation between experimental and theoretical ECD spectra seems at first glance to be less optimal with the aug-cc-pVDZ basis set than with the 6-31G* basis set. However, it should be noted that the electronic transitions predicted with B3LYP functional appear[30,31] usually at longer wavelengths than the experimentally observed transitions. As a result, the B3LYP/aug-cc-pVDZ predicted EA and ECD spectra need to be blue-shifted. Such blue shift does not appear to be necessary for predictions obtained with the lower level 6-31G* basis set, which is probably fortuitous. When such blue shift is incorporated for aug-cc-pVDZ predictions, the predicted negative ECD band at 245 nm for (*S*)-**1** matches the experimental ECD band at 212 nm for (−)-**1**. Then the predicted positive ECD band at shorter wavelength will appear below the wavelength range where experimental measurements can be performed. Examination of the predicted molecular orbital coefficients indicate that that the electronic transition giving rise to the negative ECD band predicted with both basis sets originates from S═O group and has n → π^* character.

The correlations between experimental ORD observations and theoretical ORD predictions with the 6-31G* and aug-cc-pVDZ basis sets are shown in Figure 6, panels A and B, respectively. The discrepancy among the ORD theoretical predictions obtained with two basis sets is large to the extent that the conclusions regarding structural elucidation can vary depending on which basis set is considered. This is because the ORD predictions for two conformers of (*S*)-**1** with the lower level 6-31G* basis set have opposite signs. The ORD sign predicted

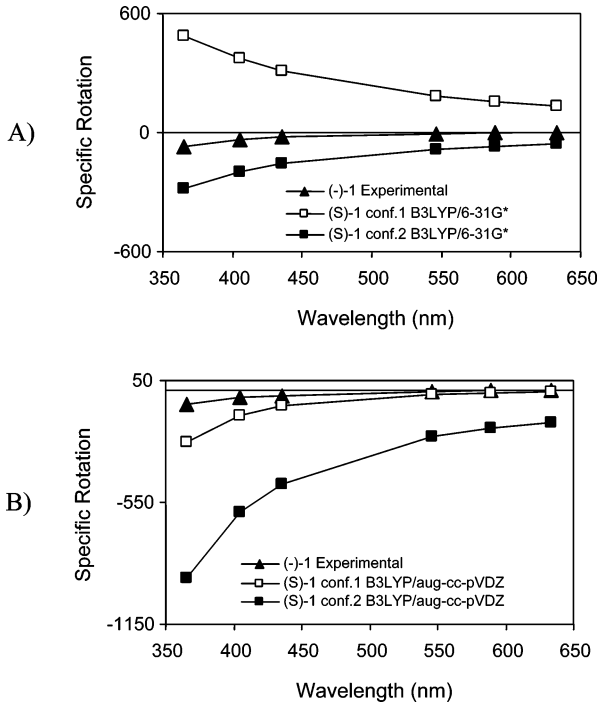

Figure 6. Comparison of ORD spectra between (−)-**1** and both conformers of (*S*)-**1** at the 6-31G* (A) and aug-cc-pVDZ (B) basis sets.

for conformer 2 of (*S*)-**1** matches the experimental ORD of (−)-**1**, whereas that for conformer 1 of (*S*)-**1** is opposite. This observation would lead to one of the two possible conclusions: either conformer 2 of (*S*)-**1** should be more populated in solution or (−)-**1** should correspond to (*R*)-configuration. On the other hand, the ORD predictions with the higher level aug-cc-pVDZ basis set for both conformers of (*S*)-**1** have the same sign as ORD of (−)-**1**, and the magnitudes of predicted ORD values for conformer 1 are in better agreement with experimental ORD magnitudes. On the basis of the previously concluded configurational assignment from VCD and ECD spectra, it can be concluded that predictions of ORD with the 6-31G* basis set are not reliable for **1**. Since ORD predictions obtained with 6-31G* and aug-cc-pVDZ basis sets are different, one might wonder if it is necessary to do calculations with an even higher level aug-cc-pVTZ basis set. However, since the conclusions from ORD predictions obtained with the aug-cc-pVDZ basis set are consistent with those from ECD, and also from VCD, predictions, it is believed that predictions with the aug-cc-pVTZ basis set may not add any new information.

The ORD observations on (*S*)-(−)-**1** also point out the inconsistency with some conclusions reported in the literature. Giorgio et al.[32] hypothesized that for molecules that exhibit the same sign for the longest wavelength ECD band and the nonresonant long-wavelength optical rotation, optical rotation calculations with a smaller 6-31G* basis set should provide correct predictions. The first longest wavelength ECD band for (−)-**1** at 212 nm has a negative sign (Figure 5), as does the ORD (Figure 6) in the nonresonant long-wavelength region (350−650 nm). Yet calculations of ORD for (*S*)-**1** with the 6-31G* basis set gave incorrect signs, directly contradicting the conclusion of Giorgio et al. Since ECD and ORD data are interrelated[33] via Kramers−Kronig transformation, ORD in the long-wavelength region can be influenced by several ECD bands in the short wavelength region. Therefore emphasis, or undue confidence, should not be placed on the correlation between

the signs of the longest wavelength ECD band and the nonresonant long-wavelength ORD.

The present observations on (*S*)-(−)-**1** also point out that it is important[20a] to use multiple chiroptical spectroscopic methods simultaneously for any given molecule. Unless multiple spectroscopic methods lead to the same conclusion, there must be some inadequacy in one or more of these methods. Since ECD and ORD are interrelated,[33] one cannot be certain of predicted results unless the conclusions reached from ECD and ORD are consistent. Although ECD predictions obtained with the 6-31G* basis support the assignment of (*S*)-(−)-**1**, the same basis set predictions of ORD concluded the opposite. This discrepancy points to the inadequacy of the 6-31G* basis set for ECD and ORD predictions for **1**. Thus, the need for simultaneous investigation of ECD and ORD for a given molecule, as pointed out recently,[34] is an important issue that should not be overlooked. Since the conclusions reached from VCD predictions with both 6-31G* and aug-cc-pVDZ basis sets about the absolute configuration and conformation of **1** are the same, VCD spectral predictions provide a benchmark against which the predictions of ECD and ORD can be compared. This observation reflects the advantages of using multiple spectroscopic methods in arriving at unambiguous conclusions on molecular structure.

Conclusions

The absolute configuration of (−)-*t*-butanesulfinamide has been determined using VCD, ECD, and ORD spectroscopic methods as (−)-(*S*). Furthermore, the predominant conformation of this molecule is determined to have S═O and NH_2 groups staggered with respect to the three methyl groups and to have amine hydrogens in gauche orientation with respect to S═O. The quality of predictions obtained for vibrational properties, namely, VA and VCD, is found to be satisfactory with the B3LYP functional and 6-31G* basis set. However, this basis set is found to be inadequate for obtaining reliable predictions of electronic properties, as reflected by ORD, but a larger aug-cc-pVDZ basis is found to provide satisfactory prediction of electronic properties. *t*-Butanesulfinamide serves as an example which invalidates the recommendation of using the 6-31G* basis set for molecules that exhibit the same sign for the long-wavelength ECD band and ORD. This molecule also emphasizes the importance of simultaneous investigation of ECD and ORD, and the use of multiple chiroptical spectroscopic methods, for reliable determination of stereochemistry.

Acknowledgment. We thank Randi Gant for participating in this work as a part of her research rotation. A teaching assistantship from Vanderbilt University (to A.G.P.) is greatly appreciated.

Supporting Information Available: Tables of VA, VCD, EA, and ECD intensities for two conformers obtained at the B3LYP/6-31G* and B3LYP/aug-cc-pVDZ levels of theory. This material is available free of charge via the Internet at http://pubs.acs.org.

References and Notes

(1) Mikolajczyk, M.; Drabowicz, J.; Kielbasinski, P. *Chiral Sulfur Reagents: Applications and Aymmetric and Stereoselective Synthesis*; CRC Press: New York, 1997.

(2) Metzner, P.; Thuillier, A. *Sulfur Reagents in Organic Synthesis*; Academic Press: London, 1994.

(3) Senanayake, C. H.; Krishnamurthy, D.; Lu, Z.; Han, Z.; Gallou, I. *Aldrichimica Acta* **2005**, *38* (3), 93−104.

(4) Davis, F. A.; Zhou, P.; Chen, B. *Chem. Soc. Rev.* **1998**, *27*, 13−18.

(5) Evans, D. A.; Faul, M. M.; Colombo, L.; Bisaha, J. J.; Clardy, J.; Cherry, D. *J. Am. Chem. Soc.* **1992**, *114*, 5977−5985.

(6) Davis, F. A.; Liu, H.; Zhou, P.; Fang, T.; Reddy, G. V.; Zhang, Y. *J. Org. Chem.* **1999**, *64*, 7559−7567.

(7) Pei, D.; Wang, Z.; Wei, S.; Zhang, Y.; Sun, J. *Org. Lett*. **2006**, *8* (25), 5913−5915.

(8) Ellman, J. A. *Pure Appl. Chem.* **2003**, *75*, 39−46.

(9) Davis, F. A.; Reddy, R. E.; Szewczyk, J. M.; Reddy, C. V.; Portonovo, P. S.; Zhang, H.; Fanelli, D.; Reddy, R. T.; Zhou, P.; Carroll, P. *J. Org. Chem*. **1997**, *62*, 2555−2563.

(10) Davis, F. A.; Fanelli, D. L. *J. Org. Chem.* **1998**, *63*, 1981−1985.

(11) Davis, F. A.; Szewczyk, J. M. *Tetrahedron Lett.* **1998**, *39*, 5951−5954.

(12) Davis, F. A.; Szewczyk, J. M.; Reddy, R. E. *J. Org. Chem.* **1996**, *61*, 2222−2225.

(13) Lefebvre, I. M.; Evans, S. A. *J. Org. Chem.* **1997**, *62*, 7532−7533.

(14) Mikolajczyk, M.; Lyzwa, P.; Drabowicz, J. *Tetrahedron: Asymmetry* **1997**, *8* (24), 3991−3994.

(15) Han, Z.; Krishnamurthy, D.; Pflum, D.; Grover, P.; Wald, S. A.; Senanayake, C. H. *Org. Lett*. **2002**, *4* (23), 4025−4028.

(16) Moreau, P.; Essiz, M.; Merour, J.; Bouzard, D. *Tetrahedron: Asymmetry* **1997**, *8* (4), 591−598.

(17) Clennan, E. L.; Chen, M.; Greer, A.; Jensen, F. *J. Org. Chem.* **1998**, *63*, 3397−3402.

(18) Bharatam, P. V.; Kaur, A.; Kaur, D. *J. Phys. Org. Chem*. **2002**, *15*, 197−203.

(19) Moree, W. J.; Van der Marel, G. A.; Liskamp, R. J. *J. Org. Chem.* **1995**, *60*, 5157−5169.

(20) For recent reviews, see: (a) Polavarapu, P. L. *Chem. Rec.* **2007**, *7*, 125−136. (b) Polavarapu, P. L. *Int. J. Quantum Chem*. **2006**, *106*, 1809−1814.

(21) (a) Liu, G.; Cogan, D. A.; Ellman, J. A. *J. Am. Chem. Soc*. **1997**, *119*, 9913−9914. (b) Liu, G.; Cogan, D. A.; Owens, T. D.; Tang, T. P.; Ellman, J. A. *J. Org. Chem.* **1999**, *64*, 1278−1284.

(22) Dragoli, D. R.; Burdett, M. T.; Ellman, J. A. *J. Am. Chem. Soc.* **2001**, *123*, 10127−10128.

(23) Wiex, D. J.; Ellman, J. A. *Org. Lett.* **2003**, *5* (8), 1317−1320.

(24) Qin, Y.; Wang, C.; Huang, Z.; Xiao, X.; Jiang, Y. *J. Org. Chem.* **2004**, *69*, 8533−8536.

(25) Huang, Z.; Zhang, M.; Wang, Y.; Qin, Y. *Synlett* **2005**, *8*, 1334−1336.

(26) Cogan, D. A.; Liu, G.; Kim, K.; Backes, B. J.; Ellman, J. A. *J. Am. Chem. Soc.* **1998**, *120* (32), 8011−8019.

(27) Shanmugam, G.; Polavarapu, P. L. *J. Am. Chem. Soc.* **2004**, *126*, 10292−10295.

(28) Frisch, M. J.; Trucks, G. W.; Schlegel, H. B.; Scuseria, G. E.; Robb, M. A.; Cheeseman, J. R.; Montgomery, J. A., Jr.; Vreven, T.; Kudin, K. N.; Burant, J. C.; Millam, J. M.; Iyengar, S. S.; Tomasi, J.; Barone, V.; Mennucci, B.; Cossi, M.; Scalmani, G.; Rega, N.; Petersson, G. A.; Nakatsuji, H.; Hada, M.; Ehara, M.; Toyota, K.; Fukuda, R.; Hasegawa, J.; Ishida, M.; Nakajima, T.; Honda, Y.; Kitao, O.; Nakai, H.; Klene, M.; Li, X.; Knox, J. E.; Hratchian, H. P.; Cross, J. B.; Adamo, C.; Jaramillo, J.; Gomperts, R.; Stratmann, R. E.; Yazyev, O.; Austin, A. J.; Cammi, R.; Pomelli, C.; Ochterski, J. W.; Ayala, P. Y.; Morokuma, K.; Voth, G. A.; Salvador, P.; Dannenberg, J. J.; Zakrzewski, V. G.; Dapprich, S.; Daniels, A. D.; Strain, M. C.; Farkas, O.; Malick, D. K.; Rabuck, A. D.; Raghavachari, K.; Foresman, J. B.; Ortiz, J. V.; Cui, Q.; Baboul, A. G.; Clifford, S.; Cioslowski, J.; Stefanov, B. B.; Liu, G.; Liashenko, A.; Piskorz, P.; Komaromi, I.; Martin, R. L.; Fox, D. J.; Keith, T.; Al-Laham, M. A.; Peng, C. Y.; Nanayakkara, A.; Challacombe, M.; Gill, P. M. W.; Johnson, B.; Chen, W.; Wong, M. W.; Gonzalez, C.; Pople, J. A. *Gaussian 03*; Gaussian, Inc.: Wallingford, CT, 2004.

(29) Wong, M. W. *Chem. Phys. Lett*. **1996**, *256*, 391−399.

(30) Bauernschmitt, R.; Ahlrichs, R. *Chem. Phys. Lett.* **1996**, *256*, 454−464.

(31) Polavarapu, P. L.; He, J.; Jeanne, C.; Ruud, K. *ChemPhysChem* **2005**, *6*, 2535−2540.

(32) Giorgio, E.; Minichino, C.; Viglione, R. G.; Zanasi, R.; Rosini, C. *J. Org. Chem*. **2003**, *68*, 5186−5192.

(33) (a) Polavarapu, P. L. *J. Phys. Chem. A* **2005**, *109*, 7013−7023. (b) Polavarapu, P. L.; Petrovic, A. G.; Zhang, P. *Chirality* **2006**, *18* (9), 723−732.

(34) Polavarapu, P. L. *Chirality* **2006**, *18*, 348−356.